

Prediction of pH, organic carbon content and effective cation exchange capacity through optical characterization of agricultural soils by near infrared multispectral images

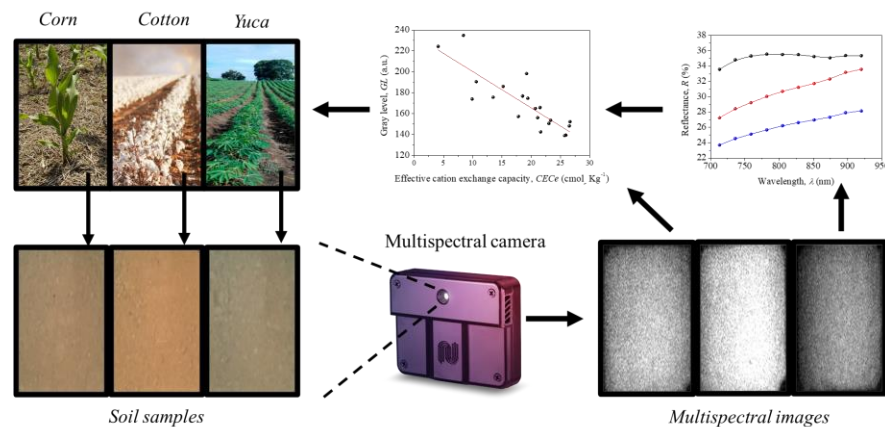
J.A. Ramírez-Rincón ¹, Manuel Palencia ^{1*}, Enrique M. Combatt ²

¹ Research Group in Science with Technological Applications (GI-CAT), Department of Chemistry, Faculty of Natural and Exact Sciences, Universidad del Valle, Cali – Colombia.

² Department of Agricultural Engineering and Rural Development, Faculty of Agricultural Sciences, Universidad de Córdoba, Montería – Colombia.

Corresponding Author: M. Palencia. E-mail: manuel.palencia@correounivalle.edu.co

Graphical Abstract



Abstract. The potential of the optical spectroscopy as a low-cost and non-invasive method, for prediction of chemical properties of agricultural soils related to their health and nutritional status has been previously demonstrated. Moreover, the advances on the imaging spectroscopy cameras have improved the usefulness of these techniques for the soil analysis, due to their ability to generate a noticeable reduction of analysis time allowing to characterize and compare different type of samples simultaneously at field and laboratory level, with a minimal consume of reagents and production of wastes. This study examines the used of multispectral imaging in near infrared region (730-920 nm) to estimate the values of pH, organic carbon content and effective cation exchange capacity in soil samples. For this, 85 soil samples grouped by their agricultural usage were collected and analyzed. In order to determine the real reflectance of each sample, the images processing required a radiometric calibration (normalization) to separate the electronic and illumination contributions on the optical signal. This allowed to identify significant relationships between reflectance values and gray level of the images with the properties of interest, obtaining Pearson's coefficients higher to 0.85 for those samples of mostly acidic properties (pH < 6.0). The developed linear models provide acceptable predictions with values of the ratio to performance deviation higher to 2.0 in all cases.

Keywords: Multispectral images, soil characterization, optical reflectance, spectral comparison.

Cite as: Ramírez-Rincón J.A., Palencia M., Combatt E. Prediction of pH, organic carbon content and effective cation exchange capacity through optical characterization of agricultural soils by near infrared multispectral images. J. Sci. Technol. Appl. 11 (2021) 4-12.
<https://doi.org/10.34294/j.jsta.21.11.70>

Accepted: 2021-10-31

Published: 2021-11-15

Paper Number: 070

Research Article



CC BY-NC-SA 4.0

This is an open access article distributed under the terms of the Creative Commons Attribution License

© MT-Pallantia Publisher 2021

1. Introduction

Soils are considered a natural non-renewable resource biologically active, compound mainly by minerals, water, air and organic matter (Bogrekci and Lee, 2005; Palacios-Orueta and Ustin, 1998; Schwanghart and Jarmer, 2011), whose properties are highly conditioned by the parent material from which it originated, its history, and the activities developed in their surface. These support several vegetable, animal and human processes, along with possess considerable importance in water and carbon cycles; therefore, there are many efforts to develop analytical and experimental methodologies that allow to estimate those properties that determine their nutritional state. In this way, traditional chemical methods result laborious and unprofitable for the analysis of huge soil samples quantity, due to requires the use of expensive reagents, where each property is obtained using specific methods (Gomez et al., 2008; Ramírez-Rincón et al., 2021; Shepherd and Walsh, 2002). Non-invasive sensing technologies based-on optical spectroscopy, along with the used of statistical and mathematical analysis tools, have been widely a used as a reliable method for simultaneously classification, estimation and characterization of structural and physicochemical properties in organic and inorganic samples (Ben-Dor and Banin, 1995; Gomez et al., 2008). This is possible through the measurement of their optical response within a specific spectral range (UV – MIR; 0.3 – 25 μm), denominated spectral footprint, which can be directly associated to sample molecular composition (Hawranek et al., 2002; Panov and Fripiat, 1998; Zaki et al., 2001). It is calculated that economical and time cost per sample, by using optical spectroscopy is only 40% compared to traditional chemical method, however it is possible reduce it up to 15% through imaging spectroscopy techniques, due to these last allow the measurement of larger surfaces instantly (O'Rourke and Holden, 2012).

As a consequence of own soil nature, which is expose continuously to spatial and temporal variations, the analytical methods must be able to provide compositional information in short time periods to be efficiently applied in agricultural industry. This, in order to know their nutritional and health state, establishing prevention and correction tools for the successful terrain management (Abbas et al., 2020; Bünemann et al., 2018; Lal, 2008). In general, the nutritional state and soils health are related to their capacity to provide the adequate conditions for plants growth, which is mediated mainly by pH levels, mineral components (associated to effective cation exchange capacity or CECe) and organic carbon content (OC), among others (Andersson et al., 2000; Curtin et al., 1998; Gentili et al., 2018; Neina, 2019).

The multi/hyperspectral spectroscopy, based on the generation of continuous and individual images in several spectral bands, provide optical and spatial information of an object in each pixel, resulting a data cube composed by two spatial dimensions (area) and one spectral (Bonifazi and Serranti, 2008). The characterization of extensive areas is developed through satellite sensors, which seek to obtain geochemical signatures in specific areas for applications in cartographic, geology, agriculture, and mineral and oil industries (Ben-Dor and Banin, 1995; Jia et al., 2016; Viscarra et al., 2006; Xu et al., 2016). Nevertheless, it is recognized that this type of sensors

presents a fault in spatial resolution, since only one pixel in the imaging can represents areas up to 900 m^2 , loosing specificity in the characterization of interest zones (Gomez et al., 2012; Manley, 2014).

The development of spectrometers of reduced size and the commercialization of this technology have popularized the use of the multi/hyperspectral cameras at laboratory and field as an alternative tool, since it allows to perform direct, fast and accurate comparisons of several samples under real conditions (Haijun et al., 2017). In agricultural applications, it has been demonstrated that imaging spectroscopy provides reliable results in the physicochemical characterization of soils, where frequently the optical information contained in the images is analyzed by using multivariate statistical techniques for spectral calibration and prediction of properties (Gmur et al., 2012; Jung et al., 2015; Stevens et al., 2008; Vaudour et al., 2016).

The studies developed in the visible and near infrared range (VNIR; 400-1000 nm) are centered mostly in those properties related with content of carbon (organic and inorganic) and moisture, due to their influence on color and optical absorption/reflection of soils in this region (Ferrando Jorge et al., 2021; Moritsuka et al., 2014; Vodyanitskii and Savichev, 2017). The above is because the absence of vibration characteristic bands, common in the IR region, limits the estimation of minerals and other important compounds for soils nutrients. This study aims to evaluate the potential of imaging spectroscopy to determine the pH, organic carbon content (OC) and effective cation exchange capacity (CECe) in agricultural soil samples, by using a multispectral camera under laboratory conditions within the spectral range 730-920 nm. The results are used to establish prediction and comparison criteria in the characterization of soils from their multispectral images and order to advance in the development of routine analyzes with lower cost, a minimal use of chemical reagents, a lower analyzing time, and a null production of residues related with the analysis procedures.

2. Materials and methods

2.1. Soil samples

Soil samples used in this study were collected to 20 cm from the surface, in different agriculture crops located in the departments of Bolivar and Cordoba (Colombia), dedicated to planting of cotton, corn and yuca. Table 1 shows the descriptive analysis of pH, CEC and OC for 85 soil samples, classified by groups according to their agriculture use (G1-G5). The pH values were obtained by the potentiometric method, using a homogeneous mixture of soil and water in relation weight/volume 1:1. The Walkley-Black method was used to determine the OC (ICONTEC, 2013), while CECe was determined by ammonium acetate method 1 N at pH 7.0 (ICONTEC, 2016, 2018).

The average (\bar{x}) pH for all groups takes similar values to the general (GN < 5.8) except in the case of G2 (7.16), which in turn has the lowest variation coefficient (CV) for this property (9%), indicating the presence of soil samples mostly alkaline (pH > 7.0). The group G1 shows the highest differences for the three properties (associated to CV values) specially in the case of OC (94%), therefore, the

higher contrast in their optical reflectance values within spectral range studied is expected. The groups G4 and G5 can be considered as the most homogeneous because the average values are similar to the GN for the three cases, and their CV are the lowest. In the case of G3, this has acid characteristics ($\text{pH} < 5.0$) and the lowest CECe values, furthermore, along with G2 presents the lower exchangeable acidity (0.52 and $0.00 \text{ cmol Kg}^{-1}$, respectively) in comparison with

Table 1. Statistical analysis of the properties for 85 soil samples in general (GN) and separated by groups (G), in terms of pH, OC, and CECe.

Group (N)		G1 (9)	G2 (26)	G3 (20)	G4 (20)	G5 (10)	GN (85)
pH (1:1)	\bar{x}	5.35	7.16	4.81	5.49	5.44	5.81
	x_{med}	4.84	7.37	4.68	5.67	5.50	5.73
	x_{min}	4.43	6.02	4.03	3.93	4.61	3.93
	x_{max}	6.97	8.17	6.63	6.58	6.60	8.17
	CV (%)	18	9%	14	13	13	20
OC (%)	\bar{x}	0.90	1.10	1.13	1.47	1.49	1.22
	x_{med}	0.39	0.92	0.88	1.54	1.66	1.26
	x_{min}	0.26	0.32	0.39	0.13	0.53	0.13
	x_{max}	2.34	2.64	2.63	2.37	2.19	2.64
	CV (%)	94	50	55	43	36	53
CECe ($\text{cmol}_c \text{ Kg}^{-1}$)	\bar{x}	15.69	20.41	10.63	18.63	15.36	16.64
	x_{med}	7.60	20.00	9.20	20.05	15.70	16.00
	x_{min}	3.10	8.3	2.10	4.10	5.70	2.10
	x_{max}	34.90	33.40	28.80	26.60	22.80	34.90
	CV (%)	84	41	70	35	38	53

Table 2. Pearson's correlation coefficients between the chemical properties associated to samples presented in Table 1, separated by group and pH level.

Properties		pH (1:1)	OC (%)	CECe ($\text{cmol}_c \text{ Kg}^{-1}$)
G1	pH (1:1)	1.000		
	OC (%)	0.855	1.000	
	CECe (cmol Kg^{-1})	0.876	0.951	1.000
G2	pH (1:1)	1.000		
	OC (%)	-0.192	1.000	
	CECe (cmol Kg^{-1})	0.340	0.343	1.000
G3	pH (1:1)	1.000		
	OC (%)	-0.206	1.000	
	CECe (cmol Kg^{-1})	0.799	0.239	1.000
G4	pH (1:1)	1.000		
	OC (%)	0.547	1.000	
	CECe (cmol Kg^{-1})	0.543	0.791	1.000
G5	pH (1:1)	1.000		
	OC (%)	0.629	1.000	
	CECe (cmol Kg^{-1})	0.714	0.874	1.000
Acid ($\text{pH} \leq 6.0$)	pH (1:1)	1.000		
	OC (%)	0.472	1.000	
	CECe (cmol Kg^{-1})	0.713	0.714	1.000
Neutral and Alkaline ($\text{pH} > 6.0$)	pH (1:1)	1.000		
	OC (%)	-0.230	1.000	
	CECe (cmol Kg^{-1})	0.248	0.352	1.000

OC: organic carbon content, CECe: effective cation exchange capacity.

G1, G3 and G4 ($3.21, 1.26, 1.10 \text{ cmol Kg}^{-1}$), therefore, the relation between their properties is expected to be different. In Table 2 are shown the Pearson's correlation coefficient (r) obtained between the pH, OC and CECe for each samples group, and separating them by the pH level (mostly acid or alkaline).

The correlation between pH and OC is positive for groups G1, G4, G5 and negative for G2 and G3. This is mediated by presence of phenols and carboxylic compounds in organic matter, which increases the availability of deionized sites at acidity conditions, and in turn the pH. In contrast, for soils of low acidity exchange properties (as G2 and G3), these compounds facilitate the release of H^+ decreasing their pH level (Andersson et al., 2000; Curtin et al., 1998). This last can be confirmed from relations obtained for the 85 soils separated by the pH level, where the values of r for these three properties are significantly major in those samples of acid properties. In general, it has been found that the relationship between the contents of pH and OC affects the dependence among OC with CECe. The above can be understood because there is a direct connection of the acidity level, mineral content and exchange cations in soil solution. Therefore, it is expected that prediction models show better results in soils of acid conditions.

2.2. Experimental setup

The Figure 1 shows the experimental setup used to generate the multispectral images. This is composed by two tungsten lamps placed in a diffusor film to homogenize the illumination over the surface of interest. The spectral images were recorded by using the Fabry-Perot Monoarch EVK Multi-Spectral Camera (Unispectral, Israel), which cover the range from 730-920 nm with 10 spectral bands of FWHM $\pm 40 \text{ nm}$. The camera was placed at 50 cm from surface (FOV $13.5 \times 13.5 \text{ cm}^2$) in normal detection (0° zenith angle), in order to improve the quality of images eliminating shadows and dark zones; moreover, an exposure time of 100 ms and gain 1.0 to avoid the saturation of signal were used. The images were individually captured for each band by snapshot mode at high resolution (1280×1040), assigning values to optical signal (radiance) from 0 to 954 according to their reflectance level (manufacturer calibration). The camera settings and the previsualization of the images were done through Unispectral software, while final analysis of information by using ENVI 5.3.

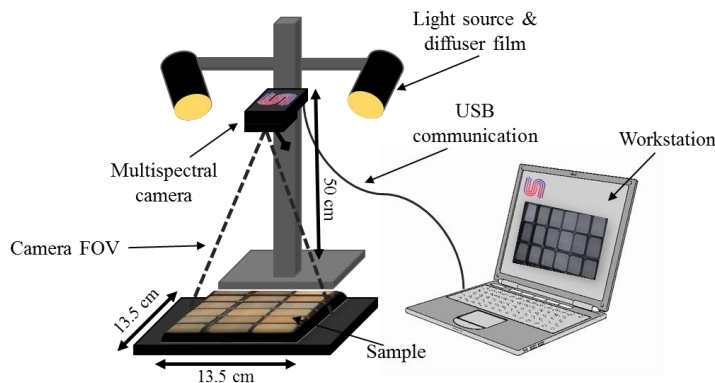


Figure 1. Scheme of the experimental setup used to generate the multispectral images

2.3. Image processing

The Figure 2a shows an image at 920 nm (grayscale) where the optical responses obtained for same an agricultural soil, under different laboratory treatments, are compared. In the first case (up), the sample has been dried at room temperature and sieved to obtain particles of diameter lower than 2.0 mm. For the other one (below), the sample has been crushed with an agate mortar to obtain smaller and more homogeneous particle sizes. Notice that even though both samples are chemically identical, the second one looks brighter, which could be associated to scattering processes related to the particles size, and consequently, the comparison of samples to determine spectral similarities is conditioned.

This is confirmed in the Figure 2b in which the optical signals obtained for the compared samples are shown. The curves correspond to average values for each spectral band over a region of interest that cover 3000 pixels, where the corresponding standard deviation has been plot as dash lines. As it is shown, the signal for sample only sieved (blue) is lower across the whole range, with a higher optical dispersion that generates an error around 11% within the measured spectrum. In the case of sieve and crush sample (red), this error decreases up 6% due to the pixels considered presents less differences as a consequence of homogeneity of surface. Similar results have been reported previously, showing that both signals provide similar information differentiated only by their level of radiance (Guo et al., 2019; Tahmasbian et al., 2018).

The growing trend of these optical signals are associated to spectral emission pattern of tungsten lamps, whereby it is mandatory to perform a normalization process of the images to determine the real reflectance values. The dependence of the obtained signals $S(\rho, \lambda)$ can be describe following the Eq. 1

$$S(\rho, \lambda) = I_0(\rho, \lambda) R(\rho, \lambda) f(\rho, \lambda), \quad (1)$$

where $I_0(\rho, \lambda)$ is the intensity of light source, which could vary for each point (ρ) over the illuminated surface, $R(\rho, \lambda)$ is the optical reflectance of the studied sample, and $f(\rho, \lambda)$ is the transference function of the camera, associated to digital transformation of light captured. The first and third factor in Eq. 1 are associated to the instruments used in the experimental setup, while the second one corresponds to the information required for characterization of the sample. Therefore, it is necessary selecting an adequate normalization signal, similar to processes developed for analysis of optical and electrical signals (Ramírez-Rincon et al., 2020; Ramírez-Rincón et al., 2018), thus, it is possible separate these dependences to determine the property of interest. In this case, it has been used a PTFE “Teflon” standard surface (reflectance 99%) that covered all FOV of multispectral camera (see Figure 1).

$$R_s(\rho, \lambda) = \frac{S_s(\rho, \lambda)}{S_{ref}(\rho, \lambda)} R_{ref}(\rho, \lambda) \quad (2)$$

The Eq. 2 corresponds to the usual normalization factor used for analysis of the multispectral images (Buddenbaum and Steffens, 2011). This indicates that the reflectance for each pixel in the 10

bands is determined dividing the optical signals for sample (S_s) and reference (S_{ref}), multiplied by a correction factor associated to PTFE surface (R_{ref}).

The Figure 3 presents the corrected (normalized) image and the corresponding reflectance for samples of Figure 2. From here, it is possible conclude that soils sieved and sieved + crush can present a difference of up to 30 % in their reflectance values and 5 % more error. Therefore, in order to generate comparable images in the 85 soil samples, all these were homogenized by sieved and crushing treatment, and their images analyzed following the Eq. 2.

3. Results and discussion

Multispectral images associated to representative samples of the minimum (Min), medium (Med) and maximum (Max) values of OC, for the soil samples described in Table 1 are shown in Figure 4a. For each case, approximately 50 g of soil has been deposited in individual racks of area 2.5x2.5 cm², which have been treated and analyzed following the methodology described in the previous section.

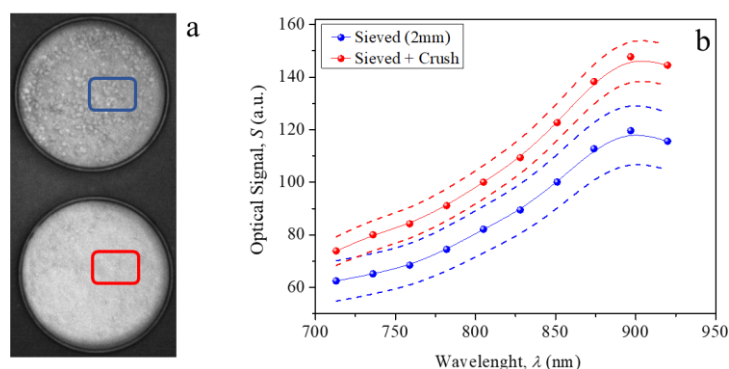


Figure 2. Comparison of the optical response (S) for identical samples under treatments of sieved (blue) and sieved + crush (red), for an image at 920 nm (a) and in the spectral range from 720 to 930 nm (b). The mean soil spectral footprint (line) and the corresponding standard deviation (dash line) show higher dispersion for the sample only sieved.

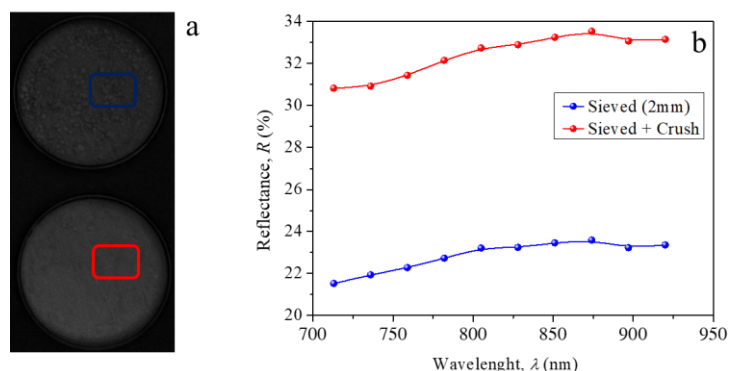


Figure 3. Comparison of the normalized optical response for identical samples, only sieved (blue) and sieved + crush (red), for an image at 920 nm (a) and for the reflectance (R) obtained in the range from 720 to 930 nm (b).

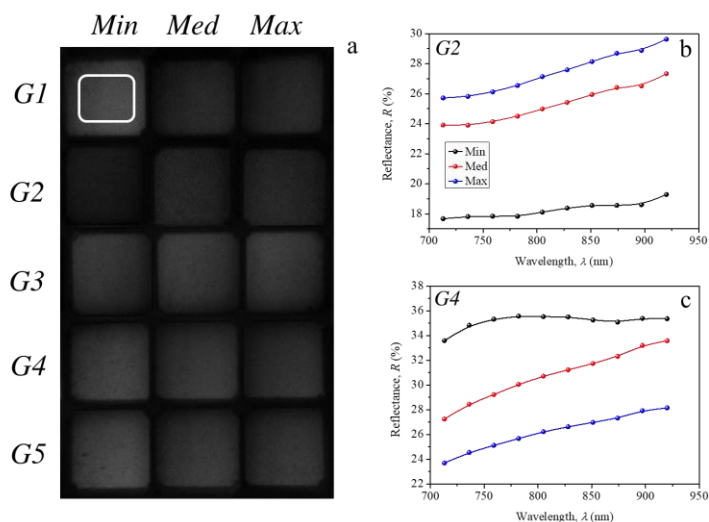


Figure 4. Normalized images at 805 nm for representative samples of the minimum (Min), medium (Med) and maximum (Max) values of organic carbon content (OC), according to data presented in Table 1 for each group (G1-G5) (a), and the corresponding average reflectance values for the groups G2 (b) and G4 (c).

Table 3. Average Pearson's correlation coefficients obtained between the reflectance values for each group of samples, and the chemical properties of interest.

Samples	pH (1:1)	OC (%)	CECe (cmol _c Kg ⁻¹)
G1-4-5	-0.748	-0.771	-0.764
G2-3	-0.382	0.281	0.394
Acid (pH ≤ 6.0)	-0.707	-0.617	-0.868
Neutral and Alkaline (pH > 6.0)	-0.532	0.189	-0.048

OC: organic carbon content, CECe: effective cation exchange capacity.

These images are represented in a digital scale from 0.0 to 1.0, that correspond to the optical signal obtained at 805 nm after normalization process. It is observed that surfaces are smooth and homogeneous in each case, whereby, the changes in bright levels can be directly related to reflectance of sample and their physicochemical properties. In Figures 4 b-c are shown the reflectance values for the samples of groups G2 and G4, which has been calculated using an average over 6000 pixels (dash square) for each spectral band. These curves summarize the typical behavior of dry soil samples, where their concavity and absolute values are conditioned by the organic compounds, minerals and iron oxides, allowing to generate prediction models in the NIR region (Buddenbaum and Steffens, 2011; Haijun et al., 2017; Stoner and Baumgardner, 1981).

According to the spectra shown in Figures 4b-c, the groups G2 and G4 present a contrary relation between the reflectance and their values of OC, positive in the first case and negative in the other one. This agrees with that found in Table 2 for the dependence OC-pH, where it has been demonstrated that those samples with acid

properties show a better correlation between the CECe, pH and OC, therefore it is possible to establish models based on optical reflectance to predict these chemical properties.

The same analytical process has been repeated with the 85 soil samples, in order to obtain their reflectance spectra and correlate them with the properties of interest through the Pearson's coefficient. The results are presented in Table 3 grouping the samples according to their chemical similarity and pH level (see Table 2).

As it is expected, those samples, where the OC, pH and CECe values are better linked (G1, G4, G5), show the higher correlations with reflectance (negative) due to the effect of pH at high acidity levels over the soil properties. In the case of G2 and G3, these correlations take low and positive values, therefore it is not possible to establish prediction models in this spectral range for samples of low exchangeable acidity. Additionally, it is observed a noticeable fall in the correlation of $R(\rho, \lambda)$ with OC for the samples of acid properties (pH < 6.0), due to each group of samples present different coloring patterns (see Figure 1) directly related with OC values, limiting the successful comparison of different types of soils.

In order to obtain images that visually represent the differences between the samples, and thus, for generating fast and reliable comparison alternatives to be used both in laboratory and field applications, it is possible to use a digital gray scale from 0 (black) to 256 (white), where the optical signal of any sample is scaled according to its reflectance values. The Figure 5a shows in gray levels (GL), the multispectral images for the samples presented in Figure 4a.

The changes in the reflectance values for a group of samples, and hence of their chemical properties when they are analyzed at the same experimental conditions, result more evident in this case since they are represented in a wider scale.

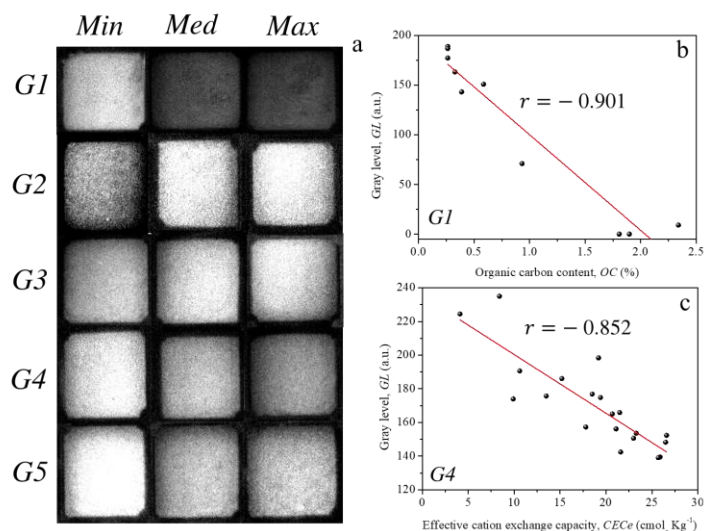


Figure 5. Grayscale images for the samples described in Figure 4 (a). Scatter plots for the organic carbon content (OC) (b) and effective cation exchange capacity (CECe) (c), with the gray levels of the images for the samples of G1 and G4, respectively.

Notice that there is a huge difference in brightness of the images for the samples Max and Min in G1, which is related to variation coefficient obtained (94 %) for the values of OC. Additionally, it can be verified that for the samples of groups G2 and G3, the reflectance decreases as the OC increases, contrary to observed for the other cases. As an example, the Figures 5 b-c show the scatter diagrams that correlate the GL with the OC and CECe values for groups G1 and G4, respectively. In both cases there is a good linear tendency between the target parameters, therefore, this type of images could be used to establish prediction and comparison criteria in the characterization of agricultural soil samples. This methodology has been proved in those samples of mostly acid properties ($\text{pH} < 6.0$), by comparison of its relative gray levels (GL_R), with the values of OC (OC_R) and CECe ($CECe_R$), taking as reference the representative samples for the minimum values of OC. The results displayed in Figure 6 demonstrate that it is possible to categorize agriculture soil samples by using simple optical

comparisons, as well to predict the values of OC (a) and CECe (b) within an acceptable analytical tolerance range for soils. In both cases, changes around 20 % in GL_N indicates differences in values of each property up to 50 %, following an almost linear tendency. The lower values of GL_R (< 0.2 not displayed) were obtained for those samples that present differences in their properties around 8 times compared to the reference. These ones correspond to soils of group G1, such as has been shown before. The reliability of gray levels for prediction of these properties has been quantified in terms of the ratio of performance to deviation (RPD), using the linear tendency (red) obtained for each case. The values of RPD between 2.0 and 2.5 indicates that prediction model used result adequate for estimation of interest properties (Chang et al., 2001; Nawar et al., 2014; Zhang et al., 2013). These results demonstrate the usefulness of optical techniques and specifically of multispectral spectroscopy, for characterization of multicomponent samples through the analysis of the generated images.

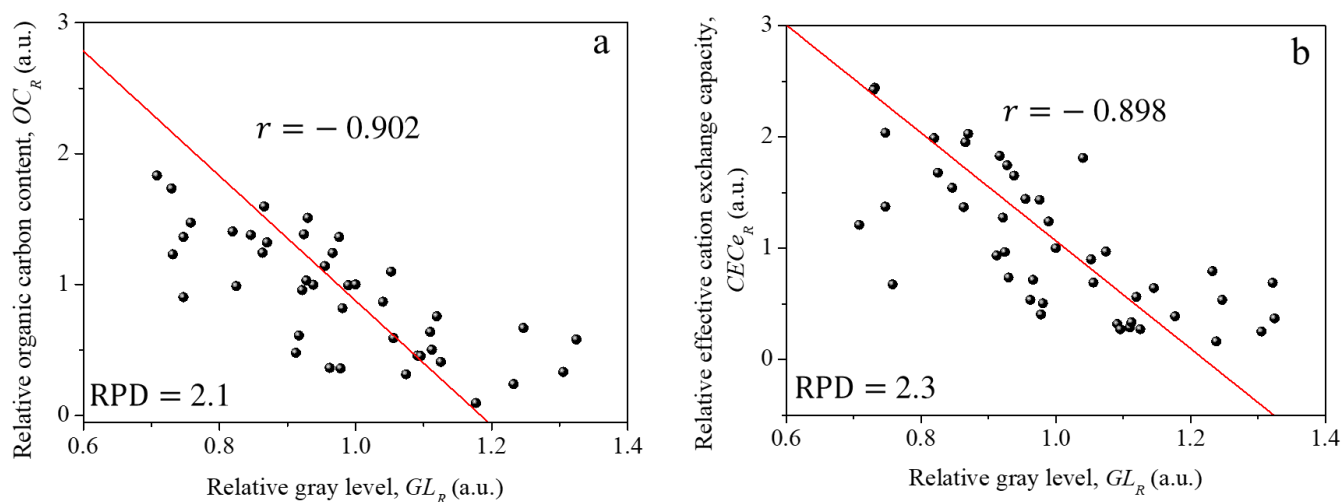


Figure 6. Scatter plots of the relative gray level (GL_R) obtained for the acid samples ($\text{pH} < 6.0$) and the relative values of organic carbon content (OC) (a) and effective cation exchange capacity (b).

4. Conclusions

In this study 85 agricultural soil samples have been characterized using the optical reflectance values, which has been obtained from multispectral images captured in 10 spectral bands within range from 730 to 920 nm. The signal processing (normalization) demonstrated a reduction of 30 % in reflectance values as a consequence of soil particle size, therefore all samples were sieved and crushed to avoid sub estimation of their optical properties. These images have been used to relate the reflectance for each soil

group with their values of pH, OC and CECe, obtaining the best results with those samples of low exchange acidity. Additionally, the multispectral images were rescaled in terms of gray levels (0 - 256) to be compared between them, allowing the generation of prediction models adequate ($\text{RPD} > 2.0$) for estimation of OC and CECe in samples of acid properties ($\text{pH} < 6.0$). These simple optical analysis processes show the useful of multi/hyperspectral spectroscopy for the rapid, low cost and accurate characterization of multicomponent samples.

⚡

Conflict interest. Authors declare that there is no conflict of interest.

Acknowledgements. Authors thanks to Ministry of Sciences of Colombia and Universidad del Valle for financial support to the project: "Fraccionamiento de las propiedades hiperespectrales de sistemas edafológicos para el diagnóstico de la fertilidad de los suelos", with C.I. 71263 and by postdoctoral fellowship No. 848-2019.

References

1. Abbas, F., Hammad, H. M., Ishaq, W., Farooque, A. A., Bakhat, H. F., Zia, Z., Fahad, S., Farhad, W., and Cerdà, A. (2020). A review of soil carbon dynamics resulting from agricultural practices. *Journal of Environmental Management*, 268, 110319. <https://doi.org/10.1016/j.jenvman.2020.110319>
2. Andersson, S., Nilsson, S. I., and Saetre, P. (2000). Leaching of dissolved organic carbon (DOC) and dissolved organic nitrogen (DON) in mor humus as affected by temperature and pH. *Soil Biology and Biochemistry*, 32(1), 1–10. [https://doi.org/10.1016/S0038-0717\(99\)00103-0](https://doi.org/10.1016/S0038-0717(99)00103-0)
3. Ben-Dor, E., and Banin, A. (1995). Near-Infrared Analysis as a Rapid Method to Simultaneously Evaluate Several Soil Properties. *Soil Science Society of America Journal*, 59(2), 364–372. <https://doi.org/10.2136/sssaj1995.03615995005900020014x>
4. Bogrekci, I., and Lee, W. S. (2005). Spectral measurement of common soil phosphates. *Transactions of the ASAE*, 48(6), 2371–2378. <https://doi.org/10.13031/2013.20076>
5. Bonifazi, G., and Serranti, S. (2008). *Hyperspectral imaging applied to complex particulate solids systems* (F. Berghmans, A. G. Mignani, A. Cutolo, P. P. Meyrueis, and T. P. Pearsall (eds.); p. 70030F). <https://doi.org/10.1117/12.781641>
6. Buddenbaum, H., and Steffens, M. (2011). Short communication: Laboratory imaging spectroscopy of soil profiles. *Journal of Spectral Imaging*. <https://doi.org/10.1255/jsi.2011.a2>
7. Bünenmann, E. K., Bongiorno, G., Bai, Z., Creamer, R. E., De Deyn, G., de Goede, R., Fleskens, L., Geissen, V., Kuyper, T. W., Mäder, P., Pulleman, M., Sukkel, W., van Groenigen, J. W., and Brussaard, L. (2018). Soil quality – A critical review. *Soil Biology and Biochemistry*, 120, 105–125. <https://doi.org/10.1016/j.soilbio.2018.01.030>
8. Chang, C.-W., Laird, D. A., Mausbach, M. J., and Hurburgh, C. R. (2001). Near-Infrared Reflectance Spectroscopy-Principal Components Regression Analyses of Soil Properties. *Soil Science Society of America Journal*, 65(2), 480–490. <https://doi.org/10.2136/sssaj2001.652480x>
9. Curtin, D., Campbell, C. A., and Jalil, A. (1998). Effects of acidity on mineralization: pH-dependence of organic matter mineralization in weakly acidic soils. *Soil Biology and Biochemistry*, 30(1), 57–64. [https://doi.org/10.1016/S0038-0717\(97\)00094-1](https://doi.org/10.1016/S0038-0717(97)00094-1)
10. Ferrando Jorge, N., Clark, J., Cárdenas, M. L., Geoghegan, H., and Shannon, V. (2021). Measuring Soil Colour to Estimate Soil Organic Carbon Using a Large-Scale Citizen Science-Based Approach. *Sustainability*, 13(19), 11029. <https://doi.org/10.3390/su131911029>
11. Gentili, R., Ambrosini, R., Montagnani, C., Caronni, S., and Citterio, S. (2018). Effect of soil ph on the growth, reproductive investment and pollen allergenicity of ambrosia artemisiifolia l. *Frontiers in Plant Science*, 9(September), 1–12. <https://doi.org/10.3389/fpls.2018.01335>
12. Gmur, S., Vogt, D., Zabowski, D., and Moskal, L. M. (2012). Hyperspectral Analysis of Soil Nitrogen, Carbon, Carbonate, and Organic Matter Using Regression Trees. *Sensors*, 12(8), 10639–10658. <https://doi.org/10.3390/s120810639>
13. Gomez, C., Lagacherie, P., and Coulouma, G. (2012). Regional predictions of eight common soil properties and their spatial structures from hyperspectral Vis–NIR data. *Geoderma*, 189–190, 176–185. <https://doi.org/10.1016/j.geoderma.2012.05.023>
14. Gomez, C., Viscarra Rossel, R. A., and McBratney, A. B. (2008). Soil organic carbon prediction by hyperspectral remote sensing and field vis-NIR spectroscopy: An Australian case study. *Geoderma*, 146(3–4), 403–411. <https://doi.org/10.1016/j.geoderma.2008.06.011>
15. Guo, L., Zhang, H., Shi, T., Chen, Y., Jiang, Q., and Linderman, M. (2019). Prediction of soil organic carbon stock by laboratory spectral data and airborne hyperspectral images. *Geoderma*, 337, 32–41. <https://doi.org/10.1016/j.geoderma.2018.09.003>

16. Haijun, Q., Xiu, J., Liu, Z., Irene Maxime, D., and Shaowen, L. (2017). Predicting sandy soil moisture content with hyperspectral imaging. *International Journal of Agricultural and Biological Engineering*, 10(6), 175–183. <https://doi.org/10.25165/j.ijabe.20171006.2614>
17. Hawranek, J. P., Wrzeszcz, W., Muszyński, A. S., and Pajdowska, M. (2002). Infrared dispersion of liquid triethylamine. *Journal of Non-Crystalline Solids*, 305(1–3), 62–70. [https://doi.org/10.1016/S0022-3093\(02\)01122-5](https://doi.org/10.1016/S0022-3093(02)01122-5)
18. ICONTEC. (2013). *Norma técnica colombiana 5403 (16) para la determinación de carbono orgánico*.
19. ICONTEC. (2016). *Norma técnica colombiana 5349 (9) para la determinación de bases cambiables: método del acetato de amonio 1N, pH 7.0*.
20. ICONTEC. (2018). *Norma técnica colombiana 5264 (16) para la determinación de pH*.
21. Jia, S., Li, H., Wang, Y., Tong, R., and Li, Q. (2016). Recursive variable selection to update near-infrared spectroscopy model for the determination of soil nitrogen and organic carbon. *Geoderma*, 268, 92–99. <https://doi.org/10.1016/j.geoderma.2016.01.018>
22. Jung, A., Vohland, M., and Thiele-Bruhn, S. (2015). Use of A Portable Camera for Proximal Soil Sensing with Hyperspectral Image Data. *Remote Sensing*, 7(9), 11434–11448. <https://doi.org/10.3390/rs70911434>
23. Lal, R. (2008). Soils and sustainable agriculture. A review. *Agronomy for Sustainable Development*, 28(1), 57–64. <https://doi.org/10.1051/agro:2007025>
24. Manley, M. (2014). Near-infrared spectroscopy and hyperspectral imaging: non-destructive analysis of biological materials. *Chem. Soc. Rev.*, 43(24), 8200–8214. <https://doi.org/10.1039/C4CS00062E>
25. Moritsuka, N., Matsuoka, K., Katsura, K., Sano, S., and Yanai, J. (2014). Soil color analysis for statistically estimating total carbon, total nitrogen and active iron contents in Japanese agricultural soils. *Soil Science and Plant Nutrition*, 60(4), 475–485. <https://doi.org/10.1080/00380768.2014.906295>
26. Nawar, S., Buddenbaum, H., Hill, J., and Kozak, J. (2014). Modeling and Mapping of Soil Salinity with Reflectance Spectroscopy and Landsat Data Using Two Quantitative Methods (PLSR and MARS). *Remote Sensing*, 6(11), 10813–10834. <https://doi.org/10.3390/rs61110813>
27. Neina, D. (2019). The Role of Soil pH in Plant Nutrition and Soil Remediation. *Applied and Environmental Soil Science*, 2019, 1–9. <https://doi.org/10.1155/2019/5794869>
28. O'Rourke, S. M., and Holden, N. M. (2012). Determination of Soil Organic Matter and Carbon Fractions in Forest Top Soils using Spectral Data Acquired from Visible-Near Infrared Hyperspectral Images. *Soil Science Society of America Journal*, 76(2), 586–596. <https://doi.org/10.2136/sssaj2011.0053>
29. Palacios-Orueta, A., and Ustin, S. L. (1998). Remote Sensing of Soil Properties in the Santa Monica Mountains I. Spectral Analysis. *Remote Sensing of Environment*, 65(2), 170–183. [https://doi.org/10.1016/S0034-4257\(98\)00024-8](https://doi.org/10.1016/S0034-4257(98)00024-8)
30. Panov, A., and Fripiat, J. J. (1998). An Infrared Spectroscopic Study of Acetone and Mesityl Oxide Adsorption on Acid Catalyst. *Langmuir*, 14(14), 3788–3796. <https://doi.org/10.1021/la971359c>
31. Ramírez-Rincón, J. A., Ares-Muzio, O., Macias, J. D., Estrella-Gutiérrez, M. A., Lizama-Tzec, F. I., Oskam, G., and Alvarado-Gil, J. J. (2018). On the use of photothermal techniques for the characterization of solar-selective coatings. *Applied Physics A*, 124(3), 252. <https://doi.org/10.1007/s00339-018-1667-5>
32. Ramirez-Rincon, J. A., Castro-Chong, A. M., Forero-Sandoval, I. Y., Gomez-Heredia, C. L., Peralta-Dominguez, D., Fernandez-Olaya, M. G., Becerril-González, J. J., Oskam, G., and Alvarado-Gil, J. J. (2020). Determination of the nonradiative conversion efficiency of lead mixed-halide perovskites using optical and photothermal spectroscopy. *Applied Optics*, 59(13), D201.

<https://doi.org/10.1364/AO.384726>

33. Ramírez-Rincón, J. A., Restrepo, D. F., and Palencia, M. (2021). The use of optical spectroscopy and hyperspectral images in the physicochemical; characterization of soils; A review. *Journal of Science with Technological Applications*, 10, 154–172. <https://doi.org/10.34294/j.jsta.21.10.69>
34. Schwanghart, W., and Jarmer, T. (2011). Linking spatial patterns of soil organic carbon to topography — A case study from south-eastern Spain. *Geomorphology*, 126(1–2), 252–263. <https://doi.org/10.1016/j.geomorph.2010.11.008>
35. Shepherd, K. D., and Walsh, M. G. (2002). Development of Reflectance Spectral Libraries for Characterization of Soil Properties. *Soil Science Society of America Journal*, 66(3), 988. <https://doi.org/10.2136/sssaj2002.0988>
36. Stevens, A., van Wesemael, B., Bartholomeus, H., Rosillon, D., Tychon, B., and Ben-Dor, E. (2008). Laboratory, field and airborne spectroscopy for monitoring organic carbon content in agricultural soils. *Geoderma*, 144(1–2), 395–404. <https://doi.org/10.1016/j.geoderma.2007.12.009>
37. Stoner, E. R., and Baumgardner, M. F. (1981). Characteristic Variations in Reflectance of Surface Soils. *Soil Science Society of America Journal*, 45(6), 1161–1165. <https://doi.org/10.2136/sssaj1981.03615995004500060031x>
38. Tahmasbian, I., Xu, Z., Boyd, S., Zhou, J., Esmaeilani, R., Che, R., and Hosseini Bai, S. (2018). Laboratory-based hyperspectral image analysis for predicting soil carbon, nitrogen and their isotopic compositions. *Geoderma*, 330, 254–263. <https://doi.org/10.1016/j.geoderma.2018.06.008>
39. Vaudour, E., Gilliot, J. M., Bel, L., Lefevre, J., and Chehdi, K. (2016). Regional prediction of soil organic carbon content over temperate croplands using visible near-infrared airborne hyperspectral imagery and synchronous field spectra. *International Journal of Applied Earth Observation and Geoinformation*, 49, 24–38. <https://doi.org/10.1016/j.jag.2016.01.005>
40. Viscarra, R., Walvoort, D. J. J., McBratney, A. B., Janik, L. J., and Skjemstad, J. O. (2006). Visible, near infrared, mid infrared or combined diffuse reflectance spectroscopy for simultaneous assessment of various soil properties. *Geoderma*, 131(1–2), 59–75. <https://doi.org/10.1016/j.geoderma.2005.03.007>
41. Vodyanitskii, Y. N., and Savichev, A. T. (2017). The influence of organic matter on soil color using the regression equations of optical parameters in the system CIE- L*a*b*. *Annals of Agrarian Science*, 15(3), 380–385. <https://doi.org/10.1016/j.aasci.2017.05.023>
42. Xu, C., Zeng, W., Huang, J., Wu, J., and van Leeuwen, W. (2016). Prediction of Soil Moisture Content and Soil Salt Concentration from Hyperspectral Laboratory and Field Data. *Remote Sensing*, 8(1), 42. <https://doi.org/10.3390/rs8010042>
43. Zaki, M. I., Hasan, M. A., and Pasupulety, L. (2001). Surface Reactions of Acetone on Al₂O₃, TiO₂, ZrO₂, and CeO₂: IR Spectroscopic Assessment of Impacts of the Surface Acid–Base Properties. *Langmuir*, 17(3), 768–774. <https://doi.org/10.1021/la000976p>
44. Zhang, T., Li, L., and Zheng, B. (2013). Estimation of agricultural soil properties with imaging and laboratory spectroscopy. *Journal of Applied Remote Sensing*, 7(1), 073587. <https://doi.org/10.1117/1.JRS.7.073587>

⌘

© MT-Pallantia Publisher (2021)